A Passive Gravitational Attitude Control System for Satellites

By B. PAUL, J. W. WEST and E. Y. YU

(Manuscript received May 28, 1963)

It is shown how the gravity-gradient effect may be utilized to design a long-lived, earth-pointing satellite attitude control system which requires no fuel supplies, attitude sensors or active control equipment. This two-body system is provided with a magnetic hysteresis damper which effectively damps out oscillations (librations) about the local vertical. The long rods, which must be extended in space from coiled up metal tapes, provide the required large moments of inertia and possess adequate rigidity and sufficient strength to endure the rigors of the extension process. The system is compatible with the requirements of multiple satellite launchings from a single last-stage vehicle. Analysis indicates that the gravitational torques are sufficient to keep the disturbing effects of solar radiation pressure, residual magnetic dipole moments, orbit eccentricity, rod curvature, eddy currents, and meteorite impacts within tolerable limits. It is believed that the high-performance, earth-pointing system described and analyzed in this paper represents an essential step in the development of high-capacity communications satellites requiring long life.

CONTENTS

I. INTRODUCTION

An earth-pointing attitude control system offers many advantages for a commercial satellite repeater. By directing the satellite's radiated power to just cover the earth, the satellite's size and weight can be minimized. For example, at a 6000-nm altitude the theoretical gain of an earth-covering conical beam is 14.5 db; however, allowance must be made for inaccuracies of the earth-pointing system and the gain that can be achieved from a practical antenna. Conservative estimates have shown that the achievable antenna gain is at least 10 db higher than with a Telstar-type isotropic antenna.* Hence, with an earth-pointing antenna, the power required from the satellite transmitter is only one-tenth that required with an isotropic antenna. This reduction in power makes the size and weight of communications satellites of high capacity (e.g., two TV channels or 600 two-way voice channels continuously operating) compatible with existing launch vehicles for orbits of interest.

In this paper we will describe a passive gravitational attitude control system (hereafter called PGAC) which provides a particularly attractive way to maintain a satellite axis pointing towards the earth. This system should have an extremely long life since it is entirely passive and requires no power and no active controls or attitude sensors. The system has been designed to be compatible with the launching of several satellites from a single launch vehicle. The importance of this feature becomes

* While the first Telstar satellite satisfied the objectives for a communications experiment, the performance was about 6 db below Bell System objectives.[1] For a higher-altitude commercial satellite, the additional 10 db would be considered essential to assist in meeting systems margins.

apparent when one considers the cost and time required to place perhaps 20 or more satellites into orbit with existing launch vehicles for a medium-altitude satellite system. Unpublished studies at Bell Telephone Laboratories have indicated that three satellites of the capacity mentioned and employing PGAC can be launched by a single Atlas-Agena vehicle in orbits of communications interest.

The most critical part of any passive earth-pointing system is the technique of damping employed to stop tumbling and limit librational motions. A unique feature of the PGAC system described herein is the employment of magnetic hysteresis damping in conjunction with a two-body system that provides large relative motion for damping purposes. Magnetic hysteresis damping is quite effective even at the slow librational rates (approximately a six-hour period at 6000-nm altitude).

PGAC employs long extensible rods to obtain appropriate moments of inertia about the three principal axes. In this respect it is similar to other passive systems[2,3] which also require long rods to obtain a sufficiently large moment of inertia in order for the gravity torque to be effective. Another feature of this PGAC system is that a single trigger or signal separates each satellite and simultaneously causes the rods to extend. This simplicity should enhance reliability of satellite separation and rod extension.

In any passive gravity-gradient orientation system, the satellite is stable with either end pointing towards the earth. In the PGAC system described here, dual antennas are proposed for each end of the satellite, and the appropriate antennas are to be activated by a simple microwave switch. Fig. 1 shows the two possible stable positions of the satellite. Antenna tests have shown that the extended rods do not substantially affect the antenna pattern; the maximum loss due to the rods is about 1 db. However, it may be possible to avoid this loss by properly orienting each satellite initially. This would require precise control of the launching vehicle orientation, satellite tumbling rate during ejection, and speed of extension of the rods.

In Section II of this paper, the dynamic principles of PGAC are described, and a general description of the system is given. Actually, two alternative configurations are described, each of which has its own advantages. Vibration analysis of the system is then given in Section III to demonstrate the validity of certain rigid body assumptions made in the dynamics analysis of the accompanying paper.[4] The stress and deformation of the rods due to dynamic loading during the extension phase and due to thermal effects are analyzed in Sections IV and V.

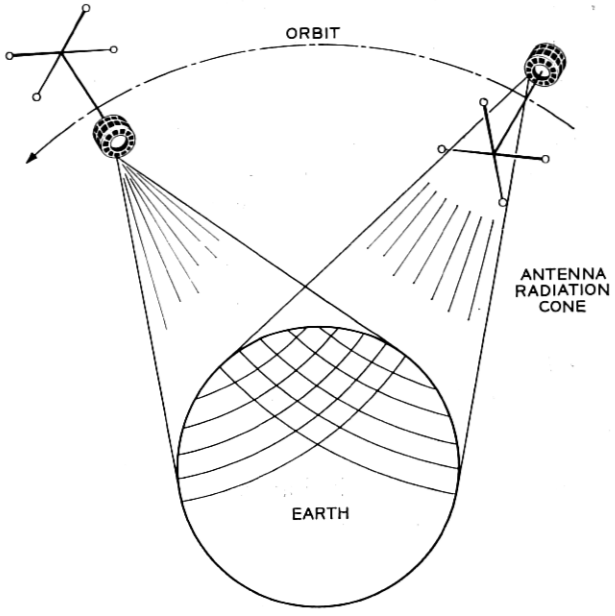

Fig. 1 — Possible satellite orientations.

Various spring designs for satellite separation associated with multiple launch are described in Section VI. The status of the hardware development and tests on the hysteresis damper unit are reviewed in Section VII. Finally, the various disturbing torques which the satellite will encounter in space are reviewed in Section VIII. It is shown that the PGAC system should remain earth-pointing within a few degrees.

Typical computer results have disclosed that for a reasonable initial tumbling rate of the satellite (1 rpm before rod extension, due to ejection from the rocket), the satellite will be earth-pointing within a few degrees of the local vertical in about 10 to 15 orbital periods. The description and discussion of PGAC in this paper is primarily for a satellite in a circular 6000-nm orbit with any inclination. However, with modifications of rod lengths and damping and spring constants, PGAC could be adapted to either higher or lower orbits.

The companion paper[4] in this issue covers the basic dynamics analysis of PGAC. The analysis includes large angle motion (as would be experienced by a satellite due to tumbling after ejection from the launch vehicle), as well as small librational motion. A complete three-dimensional analysis of the satellite motion has been formulated, and stability

criteria for the system have been determined. Other dynamics analyses of passive attitude control systems have been reported in the literature.[5,6] These analyses either have not included large angle motions or have been restricted to the pitch motion only.

II. DYNAMIC PRINCIPLES AND GENERAL DESCRIPTION OF PGAC

2.1 *Principles*

The fact that an elongated body in orbit around the earth tends to line up with the local vertical is well known.[7] Just why this should be so is most easily explained by considering a rigid dumbbell with equal tip masses. Fig. 2(a) shows a dumbbell, in orbit around the earth, whose axis makes an angle $\theta(\theta < 90°)$ with the local vertical. Since the gravitational attraction varies inversely as the square of the distance from the geocenter, the lower mass A will experience a gravity force F_A which is slightly larger than the force F_B experienced by the upper mass B.

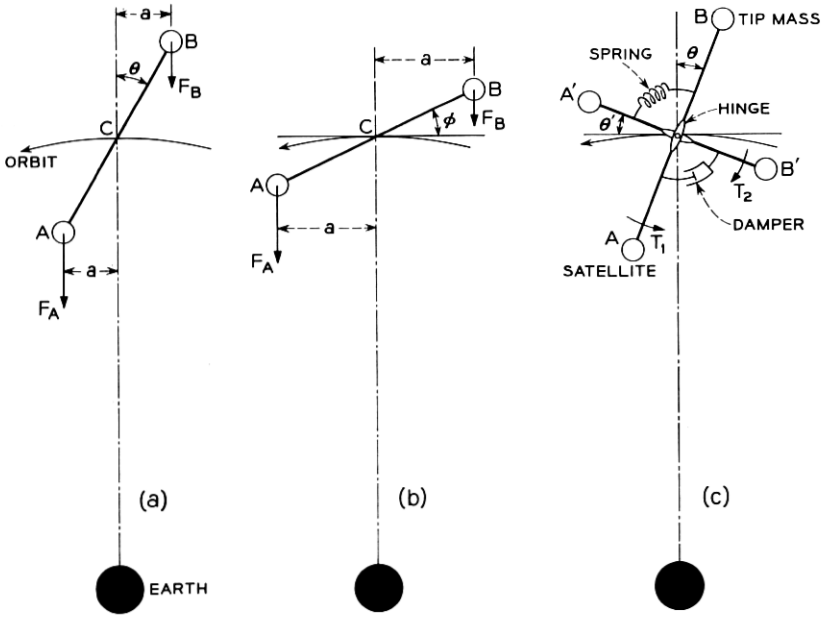

Fig. 2 — (a) Gravity forces acting on a dumbbell in orbit; (b) departure from the unstable equilibrium position; (c) system of primary and secondary dumbbells to produce damping.

The net torque about the mass center C produced by gravity forces is* $(F_A - F_B)a$ where the moment arm a is shown in Fig. 2(a). The gravity torque acts in such a direction as to diminish the angle θ. That is, it is a restoring torque which will rotate the dumbbell axis back to the local vertical. When the dumbbell becomes aligned with the local vertical, the moment arm a vanishes. Hence, the gravity torque becomes zero in the equilibrium position, $\theta = 0$. However, due to the inertia of the masses, the dumbbell does not stop in its equilibrium position but continues to rotate past it, whereupon the gravity torque reverses its direction and acts to restore the dumbbell to the local vertical. This process produces an oscillation or "libration" about the local vertical which would continue indefinitely if not damped out by some energy dissipating mechanism.

It is primarily the method of damping of the libration which distinguishes the various gravity-gradient schemes from each other. One method of damping the librations requires the use of a second dumbbell. In order to understand the function of this second body we should point out that a dumbbell is also in equilibrium (that is, no gravity torque acts upon it) when its axis is perpendicular to the local vertical. However, this equilibrium position is unstable in the sense that when the dumbbell deviates from the local horizontal by an arbitrarily small angle φ, the gravity torque $(F_A - F_B)a$ acts in such a manner (see Fig. 2b) as to increase the angle φ, i.e., to drive the system away from its (unstable) horizontal equilibrium position.

The inherent instability of a horizontal dumbbell may be used to design an efficient oscillation damper shown schematically in Fig. 2(c). In Fig. 2(c) the primary dumbbell AB is connected by means of a frictionless hinge to a secondary dumbbell A′B′. A spring is placed between the two dumbbells which keeps them crossed at right angles when the spring is not stressed. An energy dissipating device (represented in Fig. 2(c) by a piston in a close-fitting cylinder) is placed between the two dumbbells so that any relative motion of the two bodies results in a loss of mechanical energy (mechanical energy converted into heat energy). When the main dumbbell is deflected through an angle θ from the local vertical, it experiences a gravitational torque T_1 which tends to restore it to the local vertical. At the same time, because of the spring, there is a tendency for the secondary dumbbell to be carried along through an angle θ' in the same direction as the angle θ, thereby producing a gravitational torque T_2 on it which tends to increase

* Actually this is a slight oversimplification since F_A and F_B are not exactly parallel, but it adequately describes the main principle involved.

θ' still further. The net effect is that the gravity torques T_1 and T_2 tend to drive the two dumbbells in opposite direction, as shown in Fig. 2(c), thereby dissipating a relatively large amount of energy per cycle in the damping unit. The configuration shown in Fig. 2(c) will damp out oscillations in the plane of the orbit; in order to damp out oscillations perpendicular to the orbital plane, it is only necessary to add a second horizontal dumbbell which is perpendicular to the first one when its spring is unstrained. The two secondary dumbbells may be rigidly connected to each other and still provide damping in both planes of motion.

2.2 *Description*

The previous section describes the basic principles of the two-body system. In this section we discuss one method of reducing these principles to practice and describe the main features of all the major components of the system. These have reached a sufficiently high level of development for us to believe that they may be designed in detail for a specific experimental satellite.

Fig. 3 shows schematically what an actual configuration might look like. The long vertical "mast" connects the satellite to an upper "deck assembly" which serves as the tip mass for the primary "dumbbell" and as the unstable body. The deck assembly consists of two crossed dumbbells which meet at a "hinge unit" that is connected to the mast. This "hinge unit" is actually a universal joint (or Hooke's joint) which also provides elastic restoring forces (springs) and energy dissipation devices (dampers).

It should be mentioned that the deck assembly may be placed much lower on the mast rather than at its extremity as shown in Fig. 3, which illustrates a "high-deck" configuration. If the deck assembly is lowered to the vicinity of the satellite proper, the configuration will be referred to as a "low-deck" configuration (see Fig. 8 below for a schematic drawing of a low-deck configuration). From a dynamics point of view the two systems are identical. The high-deck configuration can be erected in a simple manner by the release of a single trigger which separates the satellite from the launching vehicle and simultaneously initiates extension of all rods. The low-deck arrangement has the advantage of being much stiffer structurally (see Section III) than the high-deck configuration and is much less sensitive in its response to accidental misalignment of the various rods due to initial curvatures, thermal bending, or micrometeorite impacts which might cause plastic deformation. It has the disadvantage of a more complex erection sequence (to provide

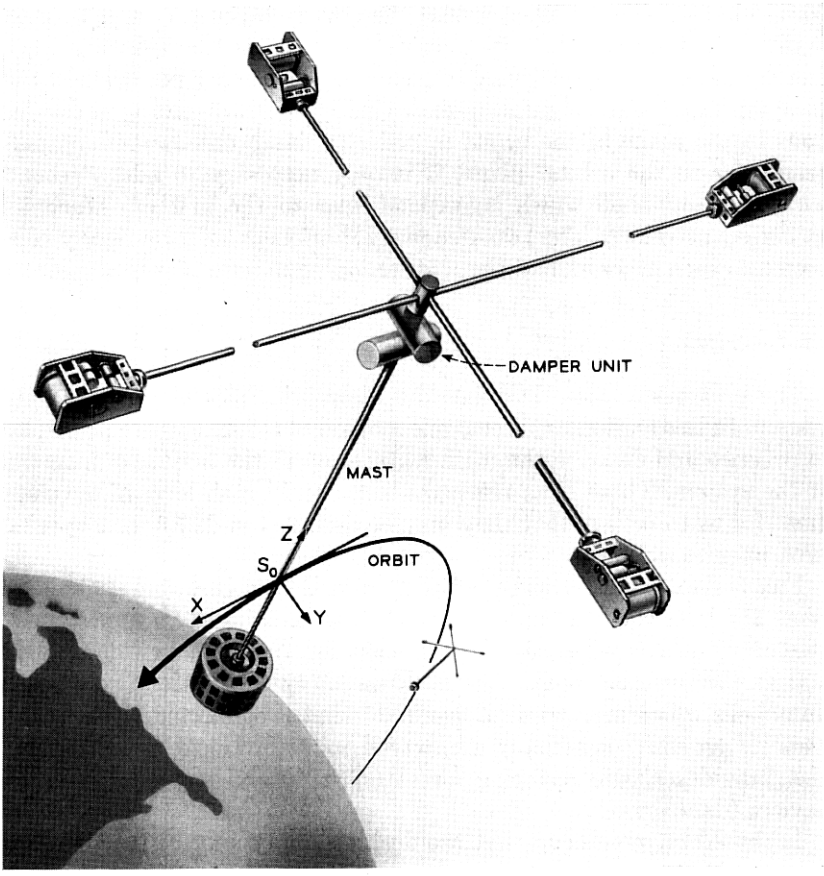

Fig. 3 — A passive gravitational attitude control (PGAC) system configuration.

clearance of the deck rods as they oscillate about the satellite body) and introduces the need to elevate a set of antennas above the height of the deck assembly in order to avoid electromagnetic difficulties.

2.2.1 *Extensible Rods*

A convenient way of erecting the rods in space is to use the STEM (Self-storing Tubular Extensible Member) units designed and developed by DeHavilland Aircraft of Canada, Ltd. These units consist of a beryllium copper tape (0.002 inch to 0.005 inch thick, and 2 inches to 5 inches wide) which is stored on a drum prior to extension, in the same

manner as a carpenter's steel tape. However, unlike the carpenter's tape, the STEM tape has been preformed so that it tends to coil into a long straight tube when unwound from the storage drum, as shown in Fig. 4. The tape has a tendency to unwind spontaneously if not restrained from doing so. In fact, it is necessary to supply a governor which limits the extension speed to a safe level or else to provide a motor which drives the tape out at a controlled rate. Whichever is used, the motor or the governor mechanism, it could be located at the extremity of the deck rod to act as part of the necessary tip mass, as shown in Fig. 3.

2.2.2 *Damper Unit*

The damper unit will permit the deck a motion of two degrees of freedom with respect to the mast in the manner of a universal joint. A proposed damper unit is shown in Fig. 5, where the two rotationally symmetric housings are rigidly fixed to one another with their axes crossed at 90°. The deck assembly is free to rotate about the axis of the upper housing while the mast is free to rotate about the axis of the lower housing, thus providing the desired two degrees of freedom. To provide the required restoring torque, the deck assembly is fixed to a rotor whose axis is aligned with that of the housing by means of two fine torsion wires (or ribbons) as shown. These wires are maintained under suitable tension by means of the leaf springs at each end of the housing. This taut wire provides the rotational restoring torque required and also serves to keep the rotor axis aligned with the axis of the housing. A slot is provided so that the connecting rod to the deck assembly may rotate through a total angle of 120° before bottoming on the end of the slot. Although it is not anticipated that the rod will ever hit its stops except for rare periods of tumbling (following injection, or collision with a micrometeorite) one may

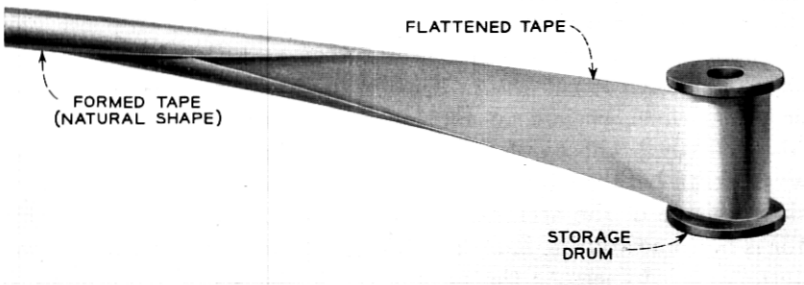

Fig. 4 — Extensible rod element.

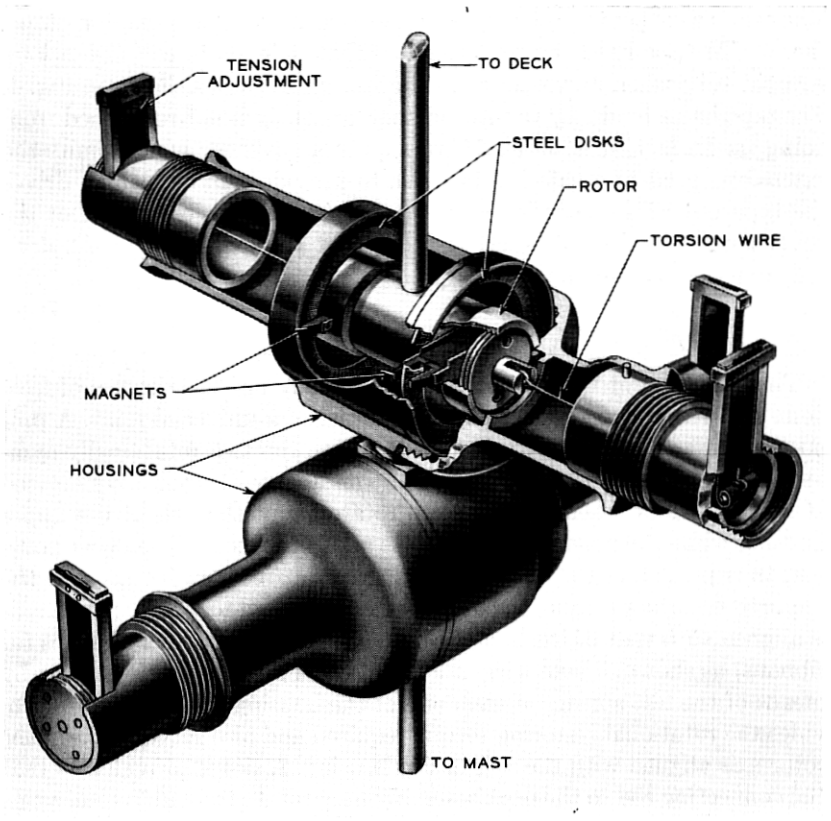

Fig. 5 — Damper unit.

design all stops so that they have no tendency to cold-weld in space. Similar stops are provided to prevent excessive lateral or axial motion of the rotor during periods of tumbling or during the launch phase.

Damping is provided by means of one or more bar magnets fixed along a diameter of the rotor. These magnets have horseshoe-shaped pole pieces which enclose an annular disk of permeable material (e.g. cold-rolled steel) whose outer rim is fixed to the housing. A small gap always exists between the faces of the pole pieces and the permeable disk by virtue of the accurate elastic suspension, and even when the rotor is bottomed during launch or tumbling, the stops maintain a predetermined clearance. As the rotor turns with respect to the housing because of satellite oscillations, the pole pieces rotate magnetic domains

in the permeable disk, thereby creating magnetic hysteresis losses. Magnetic hysteresis losses are particularly desirable because they depend essentially upon the amplitude of oscillation rather than the frequency of oscillation and have been found to be effective at the very low libration rates, which are of the same order of magnitude as the orbital frequency (a six-hour period in the case of a 6000-nm altitude).

Damper units of the type described above have been developed which provide the estimated damping torques required for 6000-nm orbits. They appear to be sufficiently rugged to withstand the launching environment and weigh approximately two pounds for the complete damper unit. The feasibility of constructing dampers for higher and lower orbits has been demonstrated. Further details of the damper development program are described in Section VII.

2.2.3 *Packaging and Multiple Launching*

Design layouts indicate that there is no difficulty in packaging a stack of several satellites within the confines of a suitable rocket vehicle in such a manner that they will withstand rocket thrust and vibrations with a minimum amount of additional structure weight. The packaging arrangement is such that each individual satellite may be ejected with the required separation speed (see Section VI). The rod extension process may be triggered by the same explosive bolt mechanism which causes satellite ejection. One possible method of achieving this is indicated in Fig. 6 which shows how the rod constraints, which are needed during the launch phase, are automatically removed when the satellite is injected into orbit.

2.2.4 *Weight Breakdown*

For a 235-lb satellite body, operating at a height of 6000 nm, computer solutions based on the work of Ref. 4 indicate that a good design is achieved if the principal moments of inertia of body 1 (principal dumbbell) are $I_1 = 3333$, $I_2 = 3333$, $I_3 = 10$ lb-ft-sec^2, and the principal moments of inertia* of body 2 (secondary rod configuration) are $I_4 = 450$, $I_5 = 1000$, $I_6 = 1450$ lb-ft-sec^2. These moments of inertia may be achieved by using a 60-ft mast rod, four 40-ft deck rods, and the mass distribution shown in Table I.

* The given values of I_4, I_5 and I_6 differ slightly from those given in the example in Ref. 4; this difference is the result of computer studies made after Ref. 4 was submitted for publication.

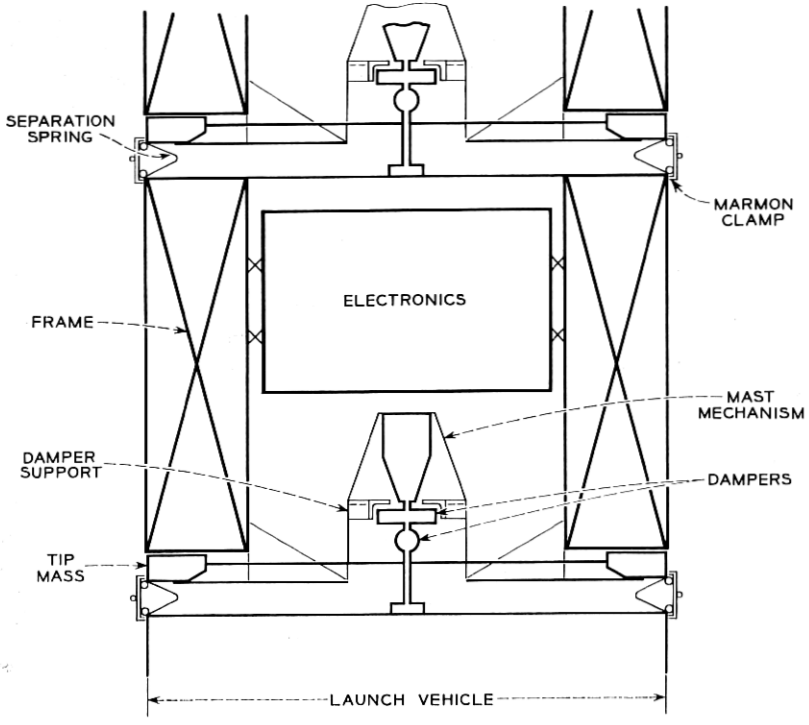

Fig. 6 — Packaging of satellites for multiple launching.

III. ELASTIC VIBRATIONS VERSUS RIGID BODY MOTION

The dynamics analyses[4] have been based on the assumption that the rods behave in an essentially rigid manner under the "gravity-free" conditions and extremely low librational angular speeds which prevail in the anticipated orbits; yet by ordinary earth-bound standards, the long thin rods would seem extremely flexible. To justify the assumption

TABLE I — MASS DISTRIBUTION

Deck tip masses	29 lbs
Deck rods	$2\frac{1}{4}$ "
Damper assembly	2 "
Mast rod	$4\frac{1}{4}$ "
Mast motor	$5\frac{1}{2}$ "
Support structure	3 "
Total	46 "

of rigid rods in the basic dynamics studies, it is necessary to estimate the bending and twisting deflections which occur in service.

It is known that under normal circumstances the entire satellite will be oscillating, or librating, at certain well defined frequencies which are of the order of orbital frequency $\Omega/2\pi$. If any part of the system, which is supposed to behave in a rigid manner, happens to have a natural vibration frequency of the order of $\Omega/2\pi$, large deformations might occur, and the results of the rigid body dynamics analyses would be open to serious question. It is the purpose of this section to show that PGAC may be designed so that its smallest natural frequency is well above the orbital frequency $\Omega/2\pi$.

It will be assumed in this section that the satellite has been aligned along the local vertical and that the elastic members of the system are undergoing small vibration with respect to a nonrotating* set of coordinate axes. In order to rigorously calculate the lowest natural frequency of such a system, it would be necessary to consider a set of coupled partial differential equations of considerable complexity. However, it will be shown in Section 3.1 below that the mast rod may be considered to be perfectly rigid in the frequency range of interest. This result enables one to find the bending and twisting frequencies of the deck assembly in a relatively simple manner (involving ordinary rather than partial differential equations) as shown in Section 3.2. Finally, it is shown in Section 3.3 that the torsional mode of the mast rod has the lowest natural frequency of interest but that this frequency is still several times higher than the orbital frequency.

3.1 *Rigidity of Mast Rod and Influence of Distributed Mass on Natural Frequencies*

Let us consider the bending vibrations of a long beam, of length L, flexural rigidity EI, and mass ρ per unit length, whose ends carry two relatively large tip masses, M_1 and M_2, but which are otherwise unconstrained, as shown in Fig. 7. Since the tip masses are so great compared to the beam mass M_3, the tips can never move too far from their equilibrium position (in comparison with the midpoint of the beam). Therefore, the principal mode shape must look somewhat as shown in Fig. 7 with nodal points very near the ends. We can thus consider the problem equivalent to that of a beam, of length $L' \approx L$, whose ends are fixed against displacement and more or less fixed against rotation, depending upon the constraints provided by the tip masses. In any case,

* This is equivalent to neglecting the curvature of the orbital path.

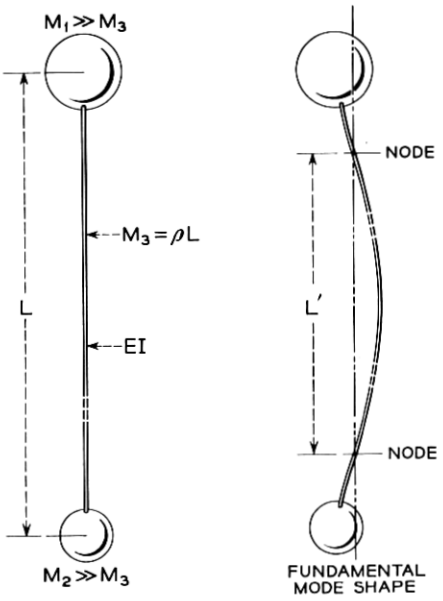

Fig. 7 — Mode shape for light beam carrying heavy tip masses.

the circular frequency p of the fundamental mode is given (Ref. 8, pp. 324–339) by

$$p = (C/L')^2\sqrt{EI/\rho} \tag{1}$$

where C is a numerical coefficient which depends upon the degree of constraint at the nodes.

Now consider two limiting cases of constraint between the mast and deck assembly. If the springs which connect the deck and mast are extremely soft, no appreciable bending moment can be transmitted to the mast from the deck, so the connection point may be treated as a hinged or simply supported end. If the tip mass at the other end has negligible moment of inertia, that end may also be considered as simply supported and the coefficient[8] $C = 3.14$ (hinged-hinged beam); but if the tip mass has an appreciable moment of inertia, the end may be considered clamped, in which case $C = 3.93$ (hinged-clamped beam). Another limiting case arises if the connecting spring is extremely stiff, in which case the deck assembly with its very large moment of inertia is almost rigidly fixed to the mast rod and essentially prevents rotation of the connected end of the mast. In this case $C = 3.93$ (clamped-hinged

beam) or $C = 4.73$ (clamped-clamped beam) accordingly as the tip mass has negligible moment of inertia or infinite moment of inertia.

We thus see that C can only undergo moderate variations despite extreme changes in the manner of end support. If one adopts the most conservative point of view and considers $C = 3.14$, (1) predicts that for a typical mast rod ($L \approx L' = 600$ in, $EI = 38{,}300$ lb in^2, $\rho = 1.51 \times 10^{-5}$ lb sec^2 in^{-2}) the fundamental mode of vibration has a frequency of $p = 1.37$ rad/sec, which is certainly well above the orbital frequency $\Omega = 0.273 \times 10^{-3}$ rad/sec for a 6000-nm orbit. Thus, we see that the influence of the distributed rod mass cannot play an important role in vibrational motions at the low frequencies of interest, and the mast rod may be considered rigid.

3.2 *Natural Frequencies of Deck Assembly*

Having shown that the mast rod is practically rigid, one may consider the satellite and mast rod a single rigid body upon which is mounted the deck assembly via the flexible joints of the damper unit. Because the deck tip masses are so great compared to the mass of the deck rods, one may neglect entirely the deck rod mass and treat the problem according to the standard "lumped mass" point of view. In particular, if one restricts attention for the time being to the low-deck configuration illustrated in Fig. 8, and notes that the center of mass* of the entire system lies fairly close to the plane of the deck assembly, one may introduce a further simplification by considering the deck assembly to be oscillating about a fixed point where the two hinge axes are assumed to cross.

In setting up the equations of motion, we shall use D'Alembert's principle, wherein each moving mass M_i is thought of as loading the structure by a system of "inertia forces": $X_i = -M_i\ddot{u}_i$, $Y_i = -M_i\ddot{v}_i$, $Z_i = -M_i\ddot{w}_i$, parallel respectively to the axes of x, y and z; and the rods are loaded by "inertia torques", $T_i = -I_{iM}\ddot{\theta}_i$. Superscript dots denote differentiations with respect to time t, in the usual Newtonian notation. To provide a more flexible and symmetrical notation, we shall frequently speak of the generalized displacements, q_i, and generalized forces, Q_i, which are related to previously defined quantities as in Table II. In this tabulation, generalized masses m_i have been defined for future reference.

Each independent deflection q_i can be found as a function of the

* The center of mass has been assumed to be unaccelerated in inertial space and for our purposes may be considered fixed.

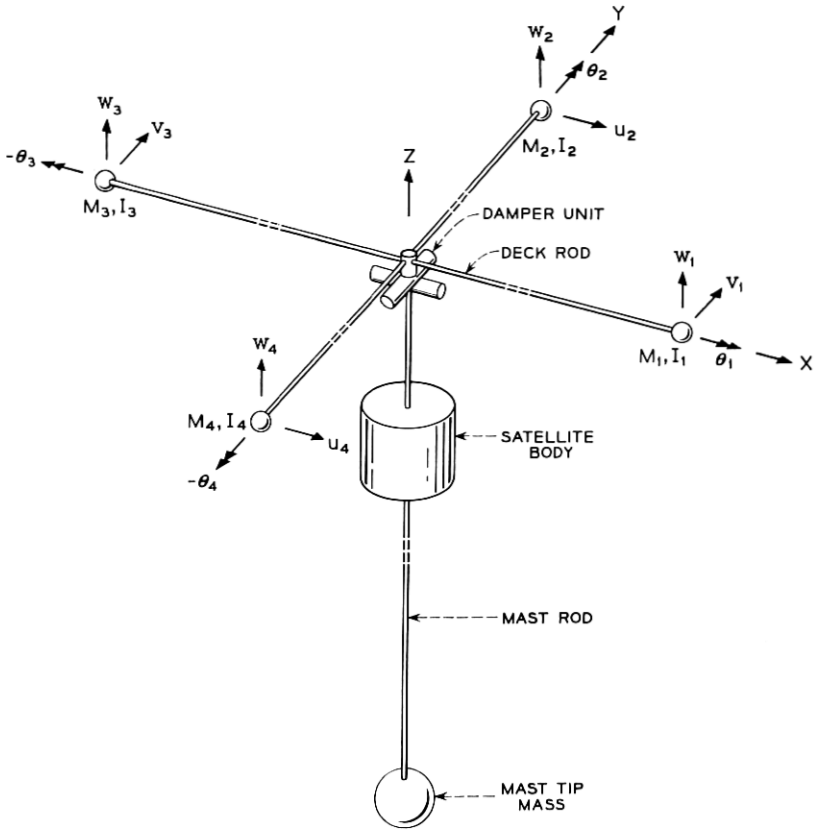

Fig. 8 — Low-deck configuration.

inertia forces applied to the system

$$q_i = \sum \frac{\partial q_i}{\partial Q_j} Q_j. \tag{2}$$

The terms $\partial q_i/\partial Q_j$ are called influence coefficients and are functions of the elastic constants and dimensions of the system. Each influence

TABLE II — GENERALIZED DISPLACEMENTS, FORCES AND MASSES

i =	1	2	3	4	5	6	7	8	9	10	11	12
q_i =	v_1	w_1	θ_i	u_2	w_2	θ_2	v_3	w_3	θ_3	u_4	w_4	θ_4
Q_i =	Y_1	Z_1	T_1	X_2	Z_2	T_2	Y_3	Z_3	T_3	X_4	Z_4	T_4
m_i =	M_1	M_1	I_{1M}	M_2	M_2	I_{2M}	M_3	M_3	I_{3M}	M_4	M_4	I_{4M}

TABLE III — LOW-DECK CONFIGURATION

Frequency p_n (rad/sec)	Most Significant Vibration
$p_1 = 0.597 \times 10^{-3}$	Oscillation of deck assembly about x (roll) axis
$p_2 = 0.643 \times 10^{-3}$	Oscillation of deck assembly about y (pitch) axis
$p_3 = p_4 = p_5 = 0.401 \times 10^{-1}$	Bending of deck rod parallel to x-axis
$p_6 = p_7 = p_8 = 0.590 \times 10^{-1}$	Bending of deck rod parallel to y-axis
$p_9 = p_{10} = 0.1373$	Twisting of deck rod parallel to x-axis
$p_{11} = p_{12} = 0.2625$	Twisting of deck rod parallel to y-axis

coefficient may be found by an elastic analysis of a statically determinate structure; for the sake of brevity, these coefficients will not be explicitly written out here.

Equation (1) may be written in the form

$$\sum_{j=1}^{12} \left[\frac{\partial q_i}{\partial Q_j} Q_j - \delta_{ij} q_i \right] = 0 \tag{3}$$

where $\delta_{ij} = 1$ for $i = j$, and $\delta_{ij} = 0$ for $i \neq j$. The symbol Q_j represents the generalized inertia force, $-m_j \ddot{q}_j$, and m_j represents the generalized mass (or moment of inertia) defined in Table II. The equations of motion are thus given by

$$\sum_{j=1}^{12} \left[\left(\frac{\partial q_i}{\partial Q_j} \right) (-m_j \ddot{q}_j) - \delta_{ij} q_i \right] = 0. \tag{4}$$

In order to solve the system of differential equations, we may assume that

$$q_i = A_i \cos (pt - \varphi) \tag{5}$$

where A_i, p and φ are as yet unknown quantities. If one substitutes (5) into (4) and follows the standard procedure,[8] one finds a twelfth-degree equation in $1/p^2$ with twelve solutions, $1/p_n^2$ for $n = 1, 2, \cdots, 12$. For these twelve (not necessarily distinct) values of p, (4) is satisfied and the assumption of (5) is justified. Equation (5) shows that the terms p_n represent the circular frequencies of the so-called natural modes of vibration. Upon the introduction of suitable numerical values, one finds the twelve natural frequencies $p_1 \cdots p_{12}$, listed in Table III, for a typical configuration designed to orbit at 6000 nm.

It may be seen from Table III that the lowest natural frequencies are those corresponding to the oscillations about the hinge-spring axes.*

* The frequency of the "rigid body" oscillations of the deck assembly about the pitch and roll hinge axes have been made intentionally close to the libration frequency in order to provide good damping. All other natural frequencies must be kept well above these values to avoid undesired resonances.

These frequencies differ from those which would be obtained with perfectly stiff deck rods by one part in 5000. The bending of deck rods has the next highest natural frequencies, which are about 70 times the pitch spring frequency. This indicates that excitation at a libration frequency ($\approx 0.5 \times 10^{-3}$ rad/sec) would not cause very large unwanted deflections any place in the structure, and that the assumption of rigid rods in the dynamics analysis is well justified for the low-deck configuration.

Although a complete vibration analysis of the high-deck configuration (shown schematically in Fig. 3) has not been made, there is no reason to believe that the natural frequencies of vibrational modes dominated by bending action will differ by orders of magnitude from similar modes in the low-deck configuration.

3.3 *Torsional Oscillations of Mast*

On the other hand, it is to be expected that the frequency of torsional vibration about the mast axis will be considerably less for the high-deck configuration. As a first approximation, one may neglect the bending deformations of the deck rods and consider the system shown in Fig. 3 as a long rod of torsional constant K_m (K_m = torque per unit twist angle) separating two rigid bodies whose moments of inertia are I_b and I_d, respectively. The angular frequency of natural oscillation is given (Ref. 8, p. 12) for such a system by

$$p = \left[K_m \frac{(I_b + I_d)}{I_b I_d}\right]^{\frac{1}{2}} \approx \left[\frac{K_m}{I_b}\right]^{\frac{1}{2}} \tag{6}$$

where the approximation follows from the fact that $I_d \gg I_b$. For a typical case of interest, one would find a torsional oscillation frequency, for the high-deck configuration, of the order of

$$p = 0.0048 \text{ rad/sec.} \tag{7}$$

This value should be compared with a libration frequency (in a so-called higher roll-yaw mode) of $p_{ry} \approx 0.00049$ rad/sec. If a somewhat more refined analysis is made, which takes into account the elasticity of the deck rods, the improved value of p differs insignificantly from the value given by (7). Although this value is smaller by an order of magnitude than the corresponding frequency of the low-deck configuration, it is still about ten times greater than the largest libration frequency. Some other comparisons between high- and low-deck arrangements have already been discussed in the introduction to Section II.

IV. STRESS AND DEFLECTION ANALYSIS OF RODS DURING EXTENSION PHASE

Since a satellite cannot be injected into orbit with absolutely zero angular velocity, in inertial space the tip masses on the extending rods will tend to cause bending and twisting of the rods during the process of extension. No attempt will be made to examine this problem in full generality, but two important representative cases will be considered. In both cases only the high-deck configuration is considered, since the low-deck configuration would seem to be at least as strong as the high-deck configuration.

Experiments[9,10] have demonstrated that a properly designed spring arrangement is capable of injecting satellites into orbit with tumbling rates below 1 rpm prior to rod extension. It is shown in this section that such rates do not cause excessive stresses or deformation in the rods during the extension process.

4.1 *Tumbling*

The satellite is idealized as shown in Fig. 9 and is assumed to be tumbling at time $t = 0$ with angular speed ω_0 about the body axis x,

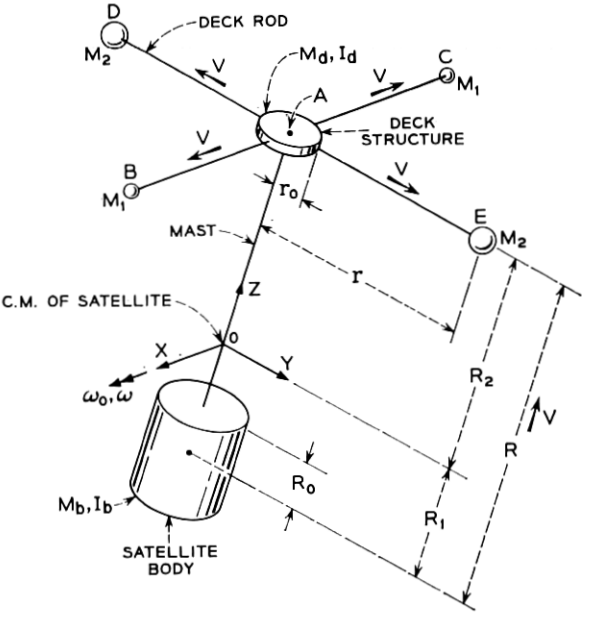

Fig. 9 — Schematic diagram of satellite during extension.

which is parallel to the deck rods carrying tip mass M_1. At time $t = 0$ both mast and deck rods begin to extend with speed v, as indicated in the sketch where r_0 represents the initial distance between the deck tip-masses and the mast axis, and R_0 equals the initial distance, measured along the mast axis, between the satellite body and the deck assembly. All mass in the deck assembly exclusive of the rods and tip masses is considered to be concentrated at the tip of the mast (point A) in the rigid body labelled "deck structure" in Fig. 9. The mass of the "deck structure" is denoted by M_d, and its moment of inertia about a centroidal axis parallel to x is denoted by I_d; similar expressions for the satellite body are denoted by M_b and I_b, respectively.

From Fig. 9 it is seen that the instantaneous distances r, R_1, and R_2 are given by

$$\begin{aligned} r &= r_0 + vt \\ R_1 &= \frac{(2M_1 + 2M_2 + M_d)(R_0 + vt)}{2(M_1 + M_2) + M_d + M_b} \\ R_2 &= \frac{M_b(R_0 + vt)}{2(M_1 + M_2) + M_d + M_b} \end{aligned} \tag{8}$$

and the instantaneous moment of inertia I of the entire system about the x-axis (passing through the instantaneous center of mass) can be shown to be

$$I(t) = I_b + I_d + \bar{M}(R_0 + vt)^2 + 2M_2(r_0 + vt)^2 \tag{9}$$

where $\bar{M}$ is defined by

$$\bar{M} = \frac{M_b(2M_1 + 2M_2 + M_d)}{2M_1 + 2M_2 + M_d + M_b}. \tag{10}$$

The initial value of I is denoted by I_0 and is found from (9) by setting $t = 0$.

We shall now assume that: (*i*) the mass of the rods is negligible; (*ii*) the hinge connection between the mast and deck assembly is rigid; (*iii*) the rods do not bend or twist (until further notice); and (*iv*) the mass center of the system is moving through inertial space with constant velocity. Under these assumptions one may apply the principle of conservation of angular momentum* to find the angular velocity ω and acceleration $\dot{\omega}$ in the form

* Although angular momentum is not strictly conserved in the presence of gravity torque, it can be shown that this effect is not significant.

$$\omega = \frac{\omega_0 I_0}{I}; \quad \dot{\omega} = \frac{-\omega_0 I_0}{I^2}\frac{dI}{dt}. \tag{11}$$

Equations (11) together with (9) fully specify the angular velocity and acceleration during the entire extension phase. The absolute acceleration $\mathbf{a}^P$ of any point P in the system may be found from the vector equation

$$\mathbf{a}^P = \frac{\delta^2\mathbf{p}}{\delta t^2} + \frac{\delta\boldsymbol{\omega}}{\delta t} \times \mathbf{p} + 2\boldsymbol{\omega} \times \frac{\delta\mathbf{p}}{\delta t} + \boldsymbol{\omega} \times (\boldsymbol{\omega} \times \mathbf{p}) \tag{12}$$

where $\mathbf{p}$ is the position vector of the point P measured from the origin shown in Fig. 9, or in terms of the unit vectors $\mathbf{i}$, $\mathbf{j}$, $\mathbf{k}$ along the body axes:

$$\mathbf{p} = p_x\mathbf{i} + p_y\mathbf{j} + p_z\mathbf{k}. \tag{13}$$

By definition:

$$\begin{aligned} \delta\mathbf{p}/\delta t &= \dot{p}_x\mathbf{i} + \dot{p}_y\mathbf{j} + \dot{p}_z\mathbf{k} \\ \delta^2\mathbf{p}/\delta t^2 &= \ddot{p}_x\mathbf{i} + \ddot{p}_y\mathbf{j} + \ddot{p}_z\mathbf{k} \\ \boldsymbol{\omega} &= \omega\mathbf{i}; \qquad \delta\boldsymbol{\omega}/\delta t = \dot{\omega}\mathbf{i}. \end{aligned} \tag{14}$$

Applying (12) successively for the five points A, B, C, D, and E shown in Fig. 9 one may find the components of acceleration $\mathbf{a}^P = a_x{}^P\mathbf{i} + a_y{}^P\mathbf{j} + a_z{}^P\mathbf{k}$ indicated in Table IV.

Table IV, together with (11), gives the absolute acceleration of all the tip masses. The D'Alembert forces acting on masses at points A, B, C, D, and E are respectively $-M_d\mathbf{a}^A$, $-M_1\mathbf{a}^B$, $-M_1\mathbf{a}^C$, $-M_2\mathbf{a}^D$, $-M_2\mathbf{a}^E$. The bending moment M_{mx} at any point z along the mast is given at any time by

$$\begin{aligned} M_{mx} = -[M_d a_y{}^A + M_1(a_y{}^B + a_y{}^C) + M_2(a_y{}^D + a_y{}^E)](R_2 - z) \\ + M_2 r(a_z{}^E - a_z{}^D) - I_d\ddot{\omega}. \end{aligned} \tag{15}$$

TABLE IV — COMPONENTS OF ACCELERATION

P (Point)	p_x	p_y	p_z	$a_x{}^P$	$a_y{}^P$	$a_z{}^P$
A	0	0	R_2	0	$-(2\dot{R}_2\omega + R_2\dot{\omega})$	$-R_2\omega^2$
B	r	0	R_2	0	$-(2\dot{R}_2\omega + R_2\dot{\omega})$	$-R_2\omega^2$
C	$-r$	0	R_2	0	$-(2\dot{R}_2\omega + R_2\dot{\omega})$	$-R_2\omega^2$
D	0	$-r$	R_2	0	$r\omega^2 - 2\dot{R}_2\omega - R_2\dot{\omega}$	$-(R_2\omega^2 + 2\dot{r}\omega + r\dot{\omega})$
E	0	r	R_2	0	$-(r\omega^2 + 2\dot{R}_2\omega + R_2\dot{\omega})$	$-R_2\omega^2 + 2\dot{r}\omega + r\dot{\omega}$

TABLE V — PARAMETERS

M_b = 286/32 lb sec²/ft	I_b = 10 or 20 lb sec² ft
M_d = 8/32 lb sec²/ft	I_d = 0.0845 lb sec² ft
M_1 = 4/32 lb sec²/ft	R_0 = 2 ft
M_2 = 9/32 lb sec² ft	r_0 = 0.75 ft
EI = 13.4 lb ft² (deck rod)	EI = 297 lb ft² (mast rod)

Similar expressions are readily written down for the bending moments at various points along the deck rods but will be omitted here for the sake of brevity. Deflections are found by noting that a tip force F produces a lateral tip deflection $\Delta_F = FL^3/(3EI)$ for a cantilever of length L and bending stiffness EI. Similarly, a tip couple M produces a lateral tip deflection of amount $\Delta_M = ML^2/(2EI)$. The net deflection is found by superposition. For a 6000-nm satellite similar to the one described in Section II, the parameters shown in Table V were used. An investigation of the complete extension history shows that for an initial tumbling rate of 0.1 rad/sec ($\approx$1 rpm) and an extension rate of $v = \frac{1}{2}$ ft/sec, the maximum stresses occur early in the process and decay rapidly thereafter; i.e., maximum moments occur before the rods have extended a distance of 2 ft. The maximum bending moments (which occur at the cantilever root) and the corresponding tip deflections (expressed as a fraction of rod length at the instant of maximum loading) are given in Table VI. Published data[11] indicate that short lengths of the mast rod could sustain a bending moment about a hundred times greater than the maximum value indicated in Table VI, and the deck rods could sustain a value about 30 times larger than the greatest tabulated value. Thus, there appears to be no "stress" problem due to tumbling.

4.2 *Spinning*

Assumptions (*i*) to (*iv*) of the previous section will be retained.

If the entire satellite spins about the mast axis with angular speed

TABLE VI — BENDING MOMENTS AND DEFLECTIONS FOR $v = \frac{1}{2}$ ft/sec; $\omega_0 = 0.1$ rad/sec

Satellite Moment of Inertia	Maximum Bending Moment, Mast	Maximum Bending Moment, Deck	Mast Tip Deflection	Deck Rod Tip Deflection
(lb sec² ft)	(ft-lb)	(ft-lb)	(Fraction of rod length)	(Fraction of rod length)
10	0.072	0.018	0.0003	0.0012
20	0.113	0.029	0.0006	0.0025

ω_0 at time $t = 0$, the deck assembly will acquire an angular speed $\dot{\theta}_d$ and the satellite body will rotate at speed $\dot{\theta}_b$. Conservation of angular momentum* requires that

$$[I_d' + 2(M_1 + M_2)(r_0 + vt)^2]\dot{\theta}_d + I_b\dot{\theta}_b = [I_d' + 2(M_1 + M_2)r_0^2 + I_b]\omega_0 \quad (16)$$

where I_d' denotes the moment of inertia of the "deck structure" about the mast axis. The torque required to produce a unit relative angular displacement between the satellite body and the deck is proportional to $(R - R_0)^{-1}$ and may be represented in the form $k/(vt)$, where k is the torsional rigidity of the mast for unit length. In other terms, the torque on the mast at any time is given by $(\theta_d - \theta_b)k/vt$; this torque is applied directly to the satellite body, so one may write

$$I_b\ddot{\theta}_b = k(\theta_d - \theta_b)/vt. \quad (17)$$

Equations (16) and (17) represent a third-order system of linear differential equations with time-dependent coefficients and with initial conditions of the form $\theta_d(0) = 0$; $\theta_b(0) = 0$; $\dot{\theta}_b(0) = \omega_0$. These equations have been integrated numerically to provide the complete response of the system during the extension phase for various sets of parameters. The solutions indicate that torsional stresses do not become excessive at any time, although the satellite body might rotate, relative to the deck assembly, by as much as 10 revolutions if an extension speed of $v = \frac{1}{2}$ ft/sec is used, and ω_0 is as high as 2 rpm. The bending stresses and deflections produced in the deck rods, under these conditions, are of the same order of magnitude (very safe) as found in the foregoing section on "tumbling." With a nonspinning final-stage vehicle it is unlikely that the initial spin rate ω_0 will reach a value as high as 1 rpm.[9,10]

4.3 *Umbrella Effect*

If all rods are being extended simultaneously, for the high-deck configuration the tip masses on the deck rods will continue to move parallel to the mast axis at the termination of the mast extension phase. This motion will continue until the cantilever bending of the deck rods has converted the tip mass kinetic energy into stored elastic energy. This effect will be referred to as the "umbrella" effect. To compute the maximum tip deflection δ_m and the maximum root bending moment M_m in the deck rods, it should be observed that a lateral tip

* Effect of gravity torque is neglected here, as in Section 4.1.

force P will produce a tip deflection $\delta_m = PL^3/3EI$, where L is the beam length and EI is the flexural rigidity. The stored strain energy U is equal to $(P/2)\delta_m$, which may be expressed as $U = 3EI\delta_m^2/2L^3$ by virtue of the linear relationship between P and δ. When the stored energy U is equated to the initial kinetic energy $(Mv^2/2)$ of a tip mass M which moves at speed v, one finds the tip deflection

$$\delta_m = v[ML^3/3EI)]^{\frac{1}{2}}. \tag{18}$$

The root bending moment M_m is found by multiplying the load $P = (3EI\delta_m/L^3)$ by the beam length L to give

$$M_m = v[3EIM/L]^{\frac{1}{2}}. \tag{19}$$

For a typical deck unit with the following parameters, $EI = 13.4$ lb ft^2, $L = 50$ ft, $M = (10/32.2)$ lb sec^2/ft, one finds that for sufficiently small values of v

$$\delta_m \text{ (ft)} = 0.983\, v \text{ (ft/sec)}$$

$$M_m \text{ (ft-lb)} = 0.500\, v \text{ (ft/sec)}.$$

Thus an extension speed of $v = \frac{1}{2}$ ft/sec would produce a bending moment of about $\frac{1}{4}$ ft-lb, which is less than the approximate allowable value of 1 ft-lb. The corresponding tip deflection of about $\frac{1}{2}$ ft is sufficiently small so that the linear bending theory used is adequate. If one wishes to find the maximum extension speed which produces a root bending moment below 1 ft-lb, it is necessary to consider a nonlinear beam theory which allows for large slopes in the deflected beam shape. An approximate treatment of this problem indicates that an extension speed of about 1.5 ft/sec would result in a root bending moment of about 1 ft-lb. Therefore, if one wishes not to exceed the load-carrying capacity of the deck rods, it is essential to keep the extension speed well below 1.5 ft/sec, or else to extend the deck rods after the mast has been fully extended.

Similar considerations show that reasonable differences in the extension speeds of the various deck rods result in tolerable loads on the mast, for practical configurations.

It should be noted that when the oscillating deck masses slam downward, they load the mast axially and tend to produce Euler-type buckling. It may readily be shown that, so long as the mast extension velocities are kept small enough to prevent overloading of the deck rods, the mast will not buckle for the configurations of interest.

V. THERMAL LOADING

The rods used in the proposed design consist of long split overlapping tubes which will experience temperature gradients due to solar heating. These temperature gradients will cause the rods to bend in such a way that the illuminated side becomes convex.

In this section, the lateral deflections of the rods due to solar heating will be calculated. In Section VIII it will be shown that these deflections have a minor influence upon the pointing accuracy of the PGAC System.

5.1 *Temperature Distribution*

It will be assumed that the rod is sufficiently long so that end effects may be ignored; hence the temperature distribution will not vary with length along the rod. Since the heat input depends upon the angle between the collimated solar rays and the axis of the rod, it is implicit in the above statement that the thermally induced curvature of the rod axis is small; this necessary requirement will be verified a posteriori in a numerical example. Confining attention to a unit length of rod as shown in Fig. 10, it may be verified that the cosine of the angle between the solar rays and the normal to a surface element located at an angle θ, measured from the outer edge of the tape, is given by

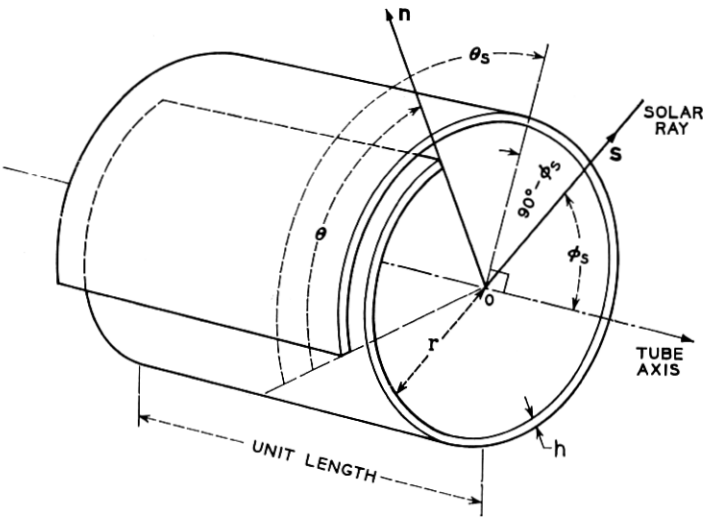

Fig. 10 — Unit length of split overlapping tube illuminated by the sun.

$$\mathbf{s}\cdot\mathbf{n} = \sin\varphi_s \cos(\theta_s - \theta) \tag{20}$$

where $\mathbf{s}$ is a unit vector pointing to the sun, $\mathbf{n}$ is a unit surface normal, φ_s is the angle between the solar rays and the tube axis, and θ_s is the angular distance from the outer free edge of the tube to the plane formed by $\mathbf{s}$ and the tube axis. The heat input per unit time on a unit area of tube surface is given by

$$q_s = a\,S \sin\varphi_s \cos^+(\theta - \theta_s) = a\,\bar{S}\cos^+(\theta - \theta_s) \tag{21}$$

where

a = absorptivity for solar radiation
S = solar constant (442 Btu/hr ft^2)
$\bar{S}$ = $S \sin\varphi_s$ = effective solar constant
$\cos^+ x = \frac{1}{2}(\cos x + |\cos x|)$ (half-rectified cosine wave).

In general, a small element of the tube of arc length $rd\theta$ (where r is the tube radius) gains heat $q_s r d\theta$, in unit time, due to solar heating; the element also gains heat $q_c r d\theta$ by conduction and loses heat $q_e r d\theta$ by emission of radiation. It will be assumed that the overlapping layers do not have an appreciable area in mutual contact. This idealization is useful because of the random nature of the actual contact areas and the uncertainties in the contact pressure and in the associated surface heat transfer coefficients. Any heat conduction which does occur between overlapping layers will tend to reduce temperature gradients and alleviate the thermal bending effect; thus, the neglect of such effects leads to a conservative analysis. Since the walls are very thin, it is permissible to assume that the temperature varies only in the circumferential direction, so that Fourier's law leads to the result

$$q_c = (\kappa h)(d^2T/r^2d\theta^2) \tag{22}$$

where κ = thermal conductivity, h = wall thickness, and T = absolute temperature. The heat loss by radiation is given by the Stefan-Boltzmann law: $q_e = \epsilon\sigma T^4$, where ϵ = hemispheric emissivity at temperature T, σ = Stefan-Boltzmann constant (1714×10^{-12} Btu/hr ft^2 (°R)^4). For simplicity, the effects of internal radiation will be neglected, so that the above expression for q_e is valid only for $0 \leqq \theta \leqq 2\pi$. The inclusion of internal radiation effects would result in reduced temperature gradients, thereby reducing the thermal bending; thus, this assumption is also conservative.

Upon summing up the three contributions to the thermal balance, one finds that

$$\frac{d^2T}{d\theta^2} - \left(\frac{\epsilon r^2}{\kappa h}\sigma\right) T^4 = -\left(\frac{r^2 a\bar{S}}{\kappa h}\right) \cos^+(\theta - \theta_s); \qquad 0 \leqq \theta \leqq 2\pi \quad (23)$$

$$\frac{d^2T}{d\theta^2} = 0; \qquad \theta > 2\pi. \quad (24)$$

Because no appreciable amount of heat can be radiated over the narrow faces (of area h per unit length) at the edges where $\theta = 0$ and $\theta = \theta_{\max}$, one may write the boundary conditions in the form $dT/d\theta = 0$ at $\theta = 0$ and $\theta = \theta_{\max}$, and observe that both T and $dT/d\theta$ must be continuous at $\theta = 2\pi$. Equation (24) implies a linear temperature distribution in the range $\theta > 2\pi$, but since $dT/d\theta$ vanishes at the edge $\theta = \theta_{\max}$, the temperature must be constant in the range $\theta > 2\pi$. In addition, continuity of $dT/d\theta$ requires that $dT/d\theta = 0$ at $\theta = 2\pi$. Thus, the temperature distribution may be found by solving the nonlinear differential equation (23), subject to the boundary condition $dT/d\theta = 0$ at $\theta = 0$, and at $\theta = 2\pi$. This problem, except for the boundary conditions, is similar to the problem treated by Charnes and Raynor[12] of a continuous (nonsplit) tube. Following their treatment, one may linearize (23) by writing

$$T = T_0 + \tau(\theta) \qquad (\tau \ll T_0) \quad (25)$$

where T_0 is the mean radiant temperature defined by

$$T_0 = [a\bar{S}/\pi\epsilon\sigma]^{\frac{1}{4}}. \quad (26)$$

Upon substitution of (25) into (23), one finds

$$\begin{gathered} d^2\tau/d\theta^2 - p^2\tau = -\beta \cos^+(\theta - \theta_s) + \lambda T_0^4 \\ d\tau/d\theta = 0 \text{ at } \theta = 0, \quad \text{and} \quad \text{at } \theta = 2\pi \end{gathered} \quad (27)$$

where

$$p = 2\sqrt{\lambda T_0^3}; \qquad \lambda = (\sigma\epsilon r^2/\kappa h); \qquad \beta = a\bar{S}r^2/\kappa h \quad (28)$$

Equation (27) may be solved by a number of standard procedures (e.g., use of Duhamel integral or of Laplace transform) which will be omitted for the sake of brevity. For a typical beryllium-copper rod, the pertinent dimensions are

$$r = 0.225 \text{ in}, \quad h = 0.002 \text{ in}, \quad \kappa = 65 \text{ Btu/hr ft}, \quad \theta_{\max} = 3\pi.$$

Representative values of absorptivity and emissivity, calculated by integration of monochromatic reflectivity measurements, are:

$$a = 0.8, \quad \epsilon = 0.3$$

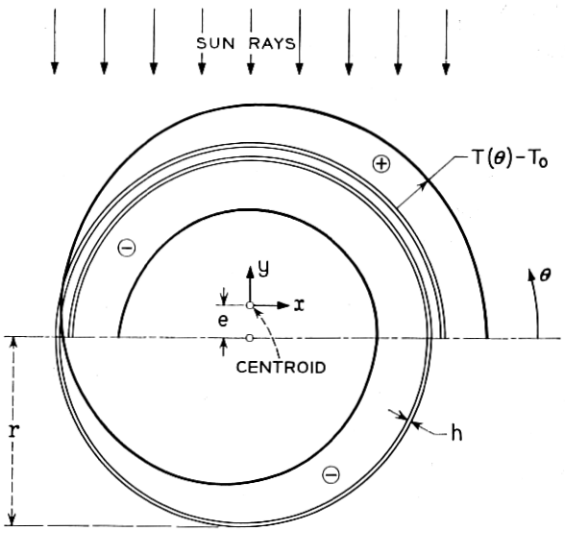

Fig. 11 — Temperature distribution in split overlapping tube (neglecting internal radiation and radial conduction effects).

where ϵ corresponds to a temperature of $T_0 = 684°R$. If the solar rays are truly normal to the rod axis, one may use $\bar{S} = S = 442$ Btu/ft^2 hr and if the rod is oriented with $\theta_s = \pi/2$, as shown in Fig. 11, the temperature distribution will be as shown in the figure, where $\tau = T - T_0$ is plotted radially outward from the tube surface for positive values and inward for negative values of τ. For this example, the temperature drops continuously from $T = 700°R$ (240°F) at $\theta = 0$ to $T = 667°R$ (207°F) at $\theta = 3\pi$.

5.2 *Thermal Bending*

Following the method used by Timoshenko and Goodier[13] for bending of a beam of rectangular cross section, one may show that the curvatures developed in the z-x plane and the z-y plane are given, respectively, by

$$\kappa_x = M_y/EI_y\,, \qquad \kappa_y = M_x/EI_x \tag{29}$$

where E is Young's modulus,

$$I_x = \int_A y^2 dA, \qquad I_y = \int_A x^2 dA \tag{30}$$

$$M_x = E\alpha \int_A \tau y dA, \qquad M_y = E\alpha \int_A \tau x dA. \tag{31}$$

In the above expressions, α represents the coefficient of thermal expansion ($\alpha = 9.4 \times 10^{-6}$ °R^{-1} for numerical example); x and y are measured from the centroid of the cross section which is located a distance e from the axis of the tube, as shown in Fig. 11; x and y have their origin at the centroid; dA represents an element of area; and the integration is made over the entire cross section.

With the temperature distribution shown in Fig. 11 (corresponding to the numerical data given above), one finds that the curvature κ_x is negligible, but κ_y is found to be

$$\kappa_y = 3.18 \times 10^{-3} \text{ ft}^{-1} \quad (R_y = 1/\kappa_y = 314 \text{ ft}).$$

It may readily be shown that one end of a rod of length L bends through an angle $\Delta\Psi = \kappa L$ with respect to the other end and deflects through a lateral distance of $\delta = (\frac{1}{2})L^2/R$. The maximum angular and lateral deviations for a 50-ft length of rod are thus seen to be $\Delta\Psi = 9.1°$, $\delta = 4.1$ ft. A similar calculation shows that $\delta = 3.5$ ft for a rod of $r = 0.45$ in and $h = 0.005$ in.

In view of the conservative nature of the heat transfer analysis used, one may estimate that the actual values of slope and deflection could easily be less than half of the computed values. In any case, the deflections do not cause excessive misalignment from the local vertical (see Section VIII), and the slopes are sufficiently small to justify the initial assumption that the heat input and temperature distribution do not vary appreciably along the axis of the rod.

VI. SPRING DESIGN FOR MULTIPLE LAUNCH

When several satellites are launched from the same rocket vehicle, it is necessary that they be injected with different velocity components along the orbit trajectory; otherwise, all the satellites will have the same period and will appear to be "bunched" together when viewed from the ground. The velocity increments required to "minimize" the undesirable effects of bunching are discussed in Ref. 14, where it is indicated that a relative speed of about 12 ft/sec between the slowest and fastest satellites is desirable for the case of four satellites in a single orbit at 6000 nm. Similar conclusions were reached in unpublished work at Bell Telephone Laboratories for the case of three simultaneously launched satellites.

Velocity increments of 12 ft/sec are readily achieved by mechanical springs. In this section we shall consider the use of ordinary helical springs and of the so-called conical disk-spring (sometimes called a Belleville spring) shown schematically in Fig. 12.

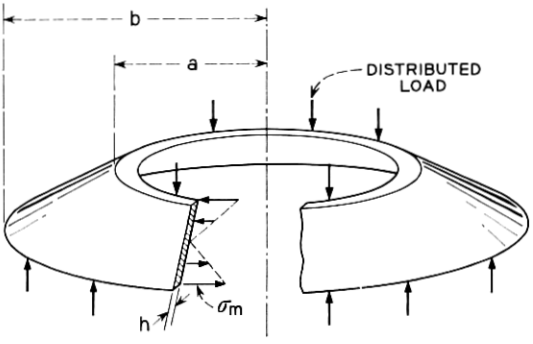

Fig. 12 — Belleville spring showing stress distribution.

It is easily shown[15] that the strain energy per unit volume u_h stored in a close-coiled helical spring with a narrow circular cross section can be expressed in the form

$$u_h = (\tfrac{1}{4})\tau_m^2/G \tag{32}$$

where τ_m is the maximum shear stress in the spring and G is the shear modulus.

In the case of a Belleville spring, the stresses are distributed[16] in an approximately linear manner over the cross section, as shown in Fig. 12, if the inequality $(b - a)/a \ll 1$ is satisfied and only small deflections are permitted. Under these conditions, it is easy to show that the strain energy per unit volume u_b is given by

$$u_b = (\tfrac{1}{6})\sigma_m^2/E \tag{33}$$

where σ_m is the maximum tensile stress in the spring and E is the modulus of elasticity. The relative energy-storing efficiencies of helical and Belleville springs may be found from (32) and (33) in the form

$$\frac{u_b}{u_h} = \left(\frac{2}{3}\right)\left(\frac{G}{E}\right)\left(\frac{\sigma_m}{\tau_m}\right)^2 \approx \left(\frac{\sigma_m}{2\tau_m}\right)^2 \tag{34}$$

where use has been made of the well-known relationship (Ref. 15, p. 60) $(E/G) = 2(1 + \nu)$ and of the fact that Poisson's ratio ν is very close to $\frac{1}{3}$ for most structural metals.

If the spring material is to be used most effectively, the stresses τ_m and σ_m should be practically equal to their respective values at the elastic limit. It is seen from (34) that the relative efficiency of Belleville springs versus helical springs depends upon the ratio of (σ_m/τ_m) at the elastic

limit. This ratio depends upon the criterion of elastic failure which governs the material. For example, a relatively ductile metal tends to yield (Ref. 16, Section 82) when either the shear stress or the octahedral shear stress reaches a critical value; for such materials it may be shown that $\sigma_m \approx 2\tau_m$. For materials with little ductility, failure generally occurs by fracture and $\sigma_m \approx \tau_m$ (Ref. 17). Therefore, (34) predicts that if the material is stressed up to its useful limit:

$$\frac{u_b}{u_h} \approx 1, \text{ for ductile materials}$$

$$\frac{u_b}{u_h} \approx \frac{1}{4}, \text{ for brittle* materials.}$$

In other terms, both Belleville and helical springs require the same volume of any given ductile metal to store equal amounts of energy; but a Belleville spring can store only $\frac{1}{4}$ the energy stored in an equal-volume helical spring made of the same relatively brittle material. Although there is a tendency towards weight saving in the use of a helical spring made of a relatively brittle material, it may well be that practical geometric considerations, reliability, and the reserve strength of ductile metals would lead one to the choice of a Belleville spring.

To show that reasonable spring weights are required for the present application, let us equate the strain energy in the spring to the kinetic energy $(\frac{1}{2})(W_{sat}/g)v^2$ required to impart a separation speed v to a satellite of weight $W_{sat}(g = 386 \text{ in/sec}^2)$. If the volume of spring material is denoted by V_{sp}, (33) leads to the result

$$U_b = u_b V_{sp} = \frac{\sigma_m^2 V_{sp}}{6E} = \frac{W_{sat} v^2}{2g} \tag{35}$$

If one uses the relationship $W_{sp} = wV_{sp}$, where W_{sp} is the total weight of the spring and w its specific weight, (35) leads to the conclusion that

$$W_{sp} = W_{sat} \frac{3v^2}{g} \left(\frac{wE}{\sigma_m^2} \right). \tag{36}$$

Equation (36) is a compact expression for the weight of a well designed Belleville spring or of a helical spring (for a material with $\sigma_m \approx 2\tau_m$). The material influences the spring weight only through the ratio (σ_m^2/wE), which may be interpreted as twice the elastic energy stored in a unit volume of the material when uniformly stressed at its maximum

* The words ductile and brittle are used in the sense that there either is or is not an appreciable amount of plastic flow between yield and fracture.

TABLE VII — MATERIAL PROPERTIES

Material	E	w	σ_m	wE/σ_m^2
	(psi)	(lb/in³)	(psi)	(in⁻¹)
(*i*) 4130 steel (HT 200,000 psi)	29×10^6	0.282	175,000	2.67×10^{-4}
(*ii*) Aluminum alloy 7075T(6)	10.4×10^6	0.101	73,000	1.97×10^{-4}
(*iii*) Titanium Alloy (Ti-6Al-6V-2Sn)	17×10^6	0.162	190,000	0.763×10^{-4}

allowable value of σ_m. Table VII shows (wE/σ_m^2) for some typical materials of interest. Thus, if one wished to impart a velocity of $v = 12$ ft/sec to a satellite weighing $W_{sat} = 280$ lb, (36) shows that with the three materials described above, the spring weight W_{sp} would be 12.1 lb, 8.8 lb, and 3.4 lb for materials (*i*), (*ii*) and (*iii*), respectively.

VII. DAMPER UNIT

The damper unit was described in qualitative terms in Section 2.2.2. In this section it will be shown in what respects the PGAC damper differs from other dampers that have been proposed in the literature, and how the damping torques and spring torques must be chosen in order to meet the system requirements outlined in the Introduction, Section I. The hardware development program for the damper units is also described.

Since the means of damping libration motions is perhaps the single most important feature which distinguishes the various attitude control systems that have been proposed by several authors, it would seem worthwhile to indicate the various methods that have been considered. These fall under two main categories: (a) velocity-dependent damping, and (b) amplitude-dependent damping.

In the first category, one finds schemes which depend upon viscous fluids[2,5,18,19] or eddy currents. It has not been demonstrated that practical difficulties concerning seals, viscosity, temperature and adverse rheological effects have been overcome in lightweight systems utilizing fluids. Calculations have shown that effective eddy-current damping requires a considerably greater weight of material than does the magnetic hysteresis unit under discussion.

In the second category of damping methods, the energy loss per cycle is independent of velocity but depends only upon the amplitude of motion. Included in this category are methods based upon Coulomb friction, internal friction,[3,6] and magnetic hysteresis, as described in Section

II of this paper. Coulomb friction (also called dry sliding friction) depends upon physical and chemical surface properties which are notoriously hard to control under conditions of high vacuum and thermal cycling; it is also difficult to control the normal force between the sliding bodies, which greatly influences the level of friction. Solid internal friction, which depends upon energy losses developed in the microstructure of the material, is quite temperature-dependent but does not depend upon unreliable surface properties and should not be unduly influenced by high vacuum.

In addition to the virtues of velocity independence, insensitivity to surface conditions, and lack of rubbing parts, the magnetic hysteresis damper proposed here has been shown to exhibit relative insensitivity to wide temperature fluctuations.

7.1 *Spring Constants*

It is shown[4] that because the deck oscillates about an unstable position of equilibrium, it is necessary to satisfy certain stability criteria. This requires that the torsional spring constants k_1 and k_2 exceed certain critical values k_1^* and k_2^* given by

$$\begin{aligned} k_1^*/I_2\Omega^2 &= 0.625 \text{ (roll)} \\ k_2^*/I_2\Omega^2 &= 1.3 \quad \text{(pitch)} \end{aligned} \tag{37}$$

for the satellite specified in Section 2.2.4, or, for 6000-nm altitude,

$$\begin{aligned} k_1^* &= 0.155 \times 10^{-3} \text{ ft-lb/rad} \\ k_2^* &= 0.324 \times 10^{-3} \text{ ft-lb/rad.} \end{aligned}$$

It is also found that k cannot be too large, since the two-body system becomes so stiff at large k that very small relative displacements between the two bodies are developed and the energy dissipation due to amplitude-dependent damping is reduced. To guarantee stability, it has been decided to keep k_1 and k_2 at least 10 per cent above their critical values. Computer studies indicate that the variation in damping time is relatively small in the range:

$$\begin{aligned} k_1 &= 0.175 \times 10^{-3} \text{ to } 0.375 \times 10^{-3} \text{ ft-lb/rad,} \\ &\qquad (k_1/I_2\Omega^2 = 0.7 \text{ to } 1.5) \\ k_2 &= 0.36 \times 10^{-3} \text{ to } 0.76 \times 10^{-3} \text{ ft-lb/rad,} \\ &\qquad (k_2/I_2\Omega^2 = 1.45 \text{ to } 3.06). \end{aligned} \tag{38}$$

From computer solutions it has been noted that if k is smaller than k^*, both the satellite body and the deck body will oscillate about cocked equilibrium positions. This verifies the stability criteria for the spring constants. If the spring constants are much larger than the maximum values given in the above ranges, the relative angular displacements become very small and little energy dissipation occurs.

7.2 *Damping Torque*

Damping torque is produced by rotational hysteresis losses obtained from relative displacement between a magnet, fixed along a diameter of the rotor, and an annular thin disk of cold-rolled steel, fixed to the housing (see Fig. 5). The magnetic fluxes of the magnet pass from the north pole of the magnet through the disk on both halves and back to the south pole, constituting a closed circuit. Except possibly for a small leakage, the unit does not act like a magnetic dipole with respect to the outside field. In the part of the disk near the poles of the magnet there is a relatively high and nonuniform magnetic field. Let the magnetic field in a magnetic domain i be H_i, and let the induced magnetization in the same domain be I_i, which is generally making an angle φ_i with H_i. The magnitude of the retarding torque can be represented by

$$\bar{T}_d = -\sum_i H_i I_i \sin \varphi_i . \tag{39}$$

The minus sign means that the torque tends to oppose the relative displacement between the disk and the magnet.

Provided that the spring constants lie in the ranges specified by (38), computer solutions have shown that there is a relatively small variation in damping time if the damping torques are in the ranges:

$$\begin{aligned} \bar{T}_{d1}/I_2\Omega^2 &= 0.12 \text{ to } 0.29 \text{ (roll)} \\ \bar{T}_{d2}/I_2\Omega^2 &= 0.16 \text{ to } 0.45 \text{ (pitch)} \end{aligned} \tag{40}$$

for the specified satellite. At 6000 nm, the numerical values of $\bar{T}_d$ are

$$\begin{aligned} \bar{T}_{d1} &= 0.30 \times 10^{-4} \text{ to } 0.72 \times 10^{-4} \text{ ft-lb} \\ \bar{T}_{d2} &= 0.40 \times 10^{-4} \text{ to } 1.12 \times 10^{-4} \text{ ft-lb.} \end{aligned} \tag{41}$$

If the damping torques are much lower than the minimum values given above, the satellite will become earth-pointing only after a large number of orbits, as indicated by computer solutions. On the other hand, if the damping torques are much larger than the maximum values, the relative displacements become small and the satellite will keep tumbling for

many orbits. In the case of large angle motion the damping time is also found to be greater for values of $\bar{T}_d$ above the ranges given in (41).

7.3 *Hardware Development Program*

Damper units have been developed whose spring constants and damping torques fall in the range given by (38) and (41). These constants are suitable for the 6000-nm satellite previously described. However, the mechanical design is such that the spring constants and damping torques may be adjusted for use with satellites at different altitudes (e.g., between 600 nm and 19,360 nm).

7.3.1 *Spring Design*

Successful torsion spring designs have evolved using both steel wires and flat beryllium-copper ribbons. The torsion springs must be under sufficient tension to prevent the lateral forces (due to gravity differentials, rotational motions, and environmental effects such as solar radiation, etc.) from deflecting the rotor laterally beyond the established clearance, thereby avoiding rubbing or sticking against the housing stops. The lateral forces have been calculated to be smaller than 10^{-3} lb for the 6000-nm satellite previously described. An axial tension force of 6 lb will be more than adequate to resist forces of this level.

Two high-strength steel wires, each of 2-in. length and 0.008-in. diameter, will meet all of the specified requirements and provide a torsional spring constant of 0.36×10^{-3} ft-lb/rad. With a suitably designed end support for the springs, a number of torsional fatigue tests have shown that the springs are capable of withstanding in excess of $\frac{1}{4}$ million cycles at an amplitude of 60°. The static axial tension was 6 to 10 lb. This number of cycles is equivalent to 5 times the expected numbers of libration periods in a 20-year useful life of the satellite.

7.3.2 *Damping Torque Test Program*

The torque-displacement relationship (e.g., T_{d1} versus α for pitch displacement) has been measured for a damper unit at angular speeds between 0.5×10^{-4} and 2×10^{-4} rad/sec (corresponding to a range of angular speeds of 0.18 Ω to 0.73 Ω at an altitude of 6000 nm). No dependence of damping torque on the angular speed has been observed in any of the tests, thereby verifying the assumption of velocity-independent magnetic hysteresis damping. Measurements have been made on a number of annular disks of various thicknesses made of cold-rolled

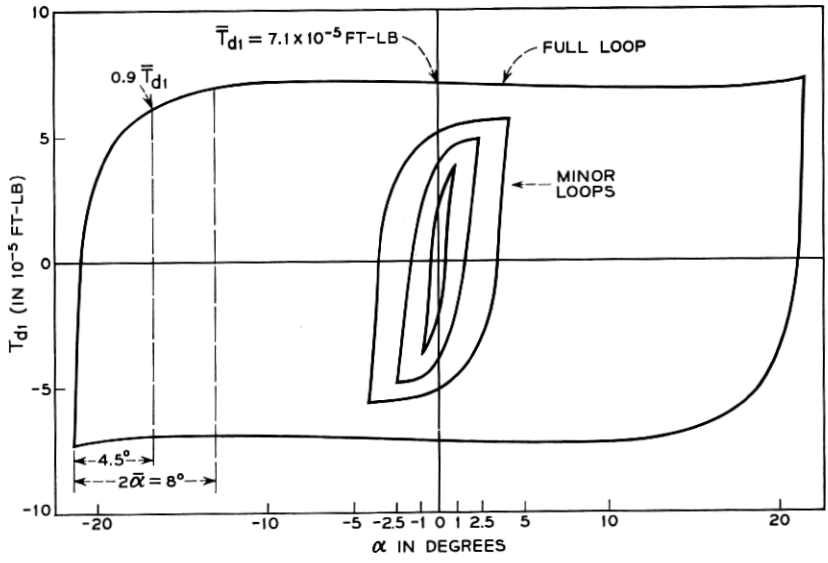

Fig. 13 — Rotational magnetic hysteresis loops.

steel, annealed and unannealed, and of V-Permendur. The maximum torque, $\bar{T}_d$, depends on the volume of the disk, the applied magnetic field and the degree of cold working of the material. A typical T_{d1}-α curve measured on an unannealed cold-rolled steel (1010) is reproduced in Fig. 13. The energy dissipated per cycle is proportional to the area enclosed by the loops in the T_{d1}-α diagram. The slanted part of the curve extends over an angular displacement, $2\bar{\alpha} \approx 8°$, as shown. When the amplitude of the oscillation motion is less than $\bar{\alpha} = 4°$, minor loops as shown in Fig. 13 will be traced out. An appreciable loop area is still obtained even when $\bar{\alpha}$ is as low as 1°.

Measurements have been made on the permeable disks after the disks have been irradiated by an electron flux of 10^{17}/cm^2, which is roughly equivalent to the highest electron radiation level anticipated within the Van Allen belt for a period of 30 years. The results indicate that electron radiation has very little effect on the damping torque. The effects of proton bombardment at a flux of 3×10^{12} protons/cm^2 have also been found insignificant on the unannealed cold-rolled steel disks of 0.004- to 0.008-inch thickness without shielding. This flux is equivalent to the highest proton radiation level at 6000 nm for a period of 6 years.

It has also been experimentally observed that the damping torque is relatively insensitive to wide temperature changes. The torque increases

only 10 per cent at −40°F and decreases only 15 per cent at +250°F, from its value at room temperature. The temperature of the damper can be controlled within much closer limits in space by appropriate coatings, if desired.

Vibration tests at a 20-g level over a wide frequency band show that the damper will withstand launch conditions.

VIII. ANALYSIS OF DISTURBANCES AND ERRORS

In this section, we shall study the nature and magnitude of disturbing torques which produce forced librational motion of a gravitationally oriented satellite. In Sections 8.1 to 8.6, calculated values are given for each disturbing torque and its corresponding libration angle.

In Section 8.7, the accumulative effects of all the disturbing torques are summarized. It will be seen that the satellite has been so designed that the gravitational torque dominates all disturbing torques at the altitudes of interest.

It is obvious that the amplitude of steady-state librational motion should be kept to a minimum in order that maximum gain can be achieved from the earth-pointing antenna. For example, the theoretical (solid angle) gain at 6000 nm is 14.5 db with no allowance for librational motion. Allowance of a conservative tolerance of 10° on an antenna half angle, to accommodate 10° libration amplitude, results in a 3-db reduction of theoretical antenna gain. However, it will be shown that the steady-state librational amplitude will be less than 10°.

8.1 *Solar Radiation Pressure*

An incident photon beam from the sun to a surface element will be partly absorbed, partly diffusely reflected and partly specularly reflected by the surface, resulting in an exertion of forces in directions normal and tangential to the surface element. These forces produce a net torque about the center of mass of the satellite. A detailed enumeration of the torques contributed by different surface elements on the two-body satellite shown in Fig. 3 indicates that a net maximum solar radiation torque of 0.5×10^{-4} ft-lb will act on the satellite. The magnitude of the gravitational torque at 6000-nm altitude is 0.13×10^{-4} ft-lb per degree of angle, θ, off the local vertical in the orbital plane for small libration angles ($T_{\theta_{max}} = \frac{3}{2}\Omega^2(I_1 - I_3) = 0.37 \times 10^{-3}$ ft-lb at $\theta = 45°$). Thus, statically the solar torque is balanced by the gravitational torque at $\theta = 4°$, when the sun is in its most unfavorable position. From computer solutions of the dynamics analysis in the pitch case, it is found that the

satellite, which is provided with damping, will perform oscillations about the local vertical of a maximum amplitude not greater than 4°. Both the static and dynamic analyses neglected the rod deflections due to solar heating, and the accumulative effects due to solar torque and rod thermal bending will be discussed in the summary, Section 8.7. To be certain that there are no effects which would cause the libration amplitude to appreciably exceed 4°, it would be necessary to perform a three-dimensional analysis.

The foregoing analysis was for a 6000-nm orbit employing the high-deck configuration. For significantly higher orbits the low-deck configuration would be preferred since it would experience less solar torque and a correspondingly smaller deviation from the local vertical.

8.2 *Residual Magnetic Dipole Moment*

The traveling-wave tube employed in a communications satellite such as the Telstar satellite contains two permanent magnets of equal size with the opposite poles placed against each other, thus constituting a quadrupole. Because of possible unequal strength of the two magnets and of inhomogeneous magnetic shielding outside of the traveling-wave tube, there would exist a net residual magnetic dipole moment in the satellite. Both the dipole and the quadrupole moments will interact with the geomagnetic field to produce torques. It can be shown that the torque produced by the quadrupole moment is only about 1 per cent of that produced by the residual dipole moment, when the moments of the two magnets are off by as little as 0.1 per cent. The magnetic moment of the Telstar satellite (produced mainly by the traveling-wave tube) was largely cancelled by the addition of compensating magnets. The residual dipole moment was 10^{-6} weber-meter, the magnitude of which does not seem to have changed much after the satellite was launched into orbit. The use of two traveling-wave tubes, as might be needed in the commercial system, would not appreciably change the satellite's residual magnetic moment.

Other magnetic dipole moments, which exist in the hysteresis damper units and the electric motors of the rod extension units, have been measured to be about 1.4×10^{-6} weber-meter (a value obtained by adding all the moments scalarly). Therefore, a total magnetic dipole moment of 2.4×10^{-6} weber-meter may be expected in the satellite. This value may be reduced by "compensating" the motor dipoles and by further refinement of the cancellation techniques used on the Telstar satellite. Assuming a maximum geomagnetic field of 2.71 amp-turn/meter (0.034 oersted) at 6000-nm altitude, we obtain a maximum torque

of about 0.65×10^{-5} newton-meter (0.48×10^{-5} ft-lb). Upon balancing this torque against the gravitational torque in the manner indicated in the preceding Section 8.1, one finds a static libration angle of 0.4°.

8.3 *Orbital Eccentricity*

The eccentricity, ϵ, of an elliptic orbit introduces a forcing torque on the satellite. If the eccentricity is not excessive, the satellite will settle down, as a result of damping, from an initial tumbling motion to a steady-state forced librational motion. In this case, the forcing torque due to eccentricity, $2\epsilon I\Omega^2 \sin(\Omega t + \varphi_0)$ (where $I = I_2$ or $= I_5$), occurs only in the equations of pitch libration. In the case of viscous damping, the steady-state pitch librational angle has been found;[20] however, because of the complexity of the resulting mathematical formulas, they will not be reproduced here. Since an analytical solution has not been obtained in the case of magnetic hysteresis damping, the steady-state libration angle of the earth-pointing body has not been evaluated exactly. However, it may be computed approximately by replacing the hysteresis damping by an equivalent viscous damping for the same energy dissipation per cycle (good only for small oscillations). In so doing, it is found that the libration amplitude $\theta \approx 3.6\epsilon$ radian, corresponding to the numerical data given in Section 2.2.4 and for spring constants and damping torques which fall in the range given in Section VII. A few computer solutions for the case of hysteresis damping indicate that $\theta \approx 5\epsilon$ radian. Guided final-stage vehicles are believed to be capable of achieving orbit eccentricities below 0.005, which would result in libration amplitude of about 1.5°.

8.4 *Meteorite Impact*

Based on Whipple's data,[21] the meteorite flux rate to a spherical surface in the neighborhood of the earth can be shown to be

$$\Phi = C/M \text{ meteorites per meter}^2 \text{ per year} \tag{42}$$

for meteorites of mass $\geqq M$ gram in the range of 10^{-11} to 10^{-1} gram. The constant C (in gram/meter^2-year) is found to be $C = 4.16 \times 10^{-5}$ according to Whipple and to be $C = 20.8 \times 10^{-5}$ according to Dubin.[22] For meteorites hitting the deck body, which is at a distance L from the center of mass of the satellite, it can be shown that the expected number of meteorite collisions per year which result in satellite tumbling is

$$\hat{N}_1 = \frac{\pi}{4} LA \frac{nvC}{\sqrt{3p}I_y\Omega} \tag{43}$$

where v is taken to be the average speed of meteorites, A to be the average surface area of the deck body (neglecting the shadowing effect of the earth), I_y is the maximum moment of inertia of the composite satellite, $p = (I_x - I_z)/I_y$ based on the composite satellite, and n is a factor determined by the momentum transfer (<1 for penetration, $= 1$ for completely inelastic impact, $= 2$ for perfectly elastic impact, and >2 for hypervelocity impact when the material is blown backward out of a nearly hemispherical crater). Equation (43) is based on an analysis of the planar pitch motion of a single rigid body satellite, which indicates that if an initial angular speed greater than $\sqrt{3p}\Omega$ is suddenly imparted to a satellite, which is already in line with the local vertical, the satellite will overcome a potential crest and turn over. Based on the result for pitch motion, the expected number of meteorite collision per year to give rise to angles of disturbance from the local vertical in the range from θ_1 to θ_2 ($\leqq 90°$) has been found to be

$$\hat{N}_2 = \frac{\pi}{4} LA \frac{nvC}{\sqrt{3p} I_y \Omega} \left(\frac{1}{\sin \theta_1} - \frac{1}{\sin \theta_2} \right). \tag{44}$$

Both (43) and (44) were derived in a simple manner by approximating the deck as a spherical body. A more exact result can be obtained if the meteorite flux rate is defined with respect to the projected area of a body. In this case the resulting expressions for $\hat{N}_1$ and $\hat{N}_2$ are similar to (43) and (44), respectively, except that the coefficient $(\pi/4)LA$ is replaced by complicated integrals involving the projected area element of various bodies and its distance from the mass center of the satellite.

Numerical values of $\hat{N}$ given in (43) and (44) calculated for the two-body satellite with $C = 4.16 \times 10^{-5}$ are tabulated in Table VIII, from which it is noted that the expected number of turnovers is 0.044 per year (or once in about 23 years). If $C = 20.8 \times 10^{-5}$ is used, based on Dubin's[22] data, all values of $\hat{N}$ in Table VIII should be multiplied by a factor of 5, and the expected turnover rate is 0.22 per year or once in about 4.5 years. These disturbances will be hysteretically damped down to a librational motion with amplitude of 5° in a reasonably short time. For example, computer solutions indicate that the pitch amplitude will be reduced from 45° to 5° in two to four orbital periods. In view of the uncertainty of the meteorite flux rate, all numerical values calculated in this section are to be interpreted as order of magnitude estimates.

8.5 *Cocked Angle Due to Rod Deflections*

The extensible rods will be bent in a natural way and due to the thermal effects, as analyzed in Section V. Consequently, the axes of principal

moments of inertia of both bodies will deviate from their positions in the case of perfectly straight rods, and the center of mass of the composite satellite will not lie in the mast rod. As a result, the two bodies may not be perpendicular to each other (or the springs between them may not be in a neutral position) and the desired earth-pointing axis of the satellite may be off from the local vertical by a small cocked angle when the satellite is in a stable equilibrium position. Techniques have been developed for measuring rod straightness so that the natural rod bending in a gravity-free condition will not exceed a predetermined value. It has been found possible to select rods so that the rod bending will not exceed 1 foot for a rod length of 60 feet. This cocked angle could be evaluated if we could find the position vector of the hinge joint in the distorted configuration. A general error analysis has not been made, since it is not known a priori in what way the rods might be deflected. Based on the case of pitch libration, it is found that a deflection of 1 ft of a 60-ft long mast rod will cause a cocked angle of about 0.7° in the case of the high-deck configuration. Assuming that the lateral tip deflections of both the mast and deck rods occur in the same direction, the total cocked angle will be approximately 1.5°. For the case of the low-deck configuration, the cocked angle would be appreciably less.

Rod bending can be caused by solar heating. As has been covered in Section 5.2, the deflection for a 50-ft long rod is expected to be about 2 feet when the sun is perpendicular to the rod. There is a cumulative effect due to the mast and one pair of deck rods when the tips all bend away from the sun during certain periods of the year. The cumulative effects of these rods being bent produce a maximum cocked angle of 3°. This cocked angle can be reduced to less than 1° by silver-plating the rod exterior (the low absorptivity of silver, $\alpha \approx 0.1$, would significantly reduce thermal rod bending due to a reduction of temperature differential across the rod cross section). As will be discussed in the summary, Section 8.7, the effects of rod bending and solar torques are not additive.

8.6 *Miscellaneous Torques*

Torques due to self-gravity and eddy currents have been found to be much smaller than those discussed above. It can be shown that the self-gravity torque acting on one body due to the attraction of the other body is negligibly small compared to the gravitational torque at the altitude of interest. This is due to the fact that the sizes of the two bodies are not significantly different and that their masses are much smaller than that of the earth. Eddy-current losses induced in the conducting

materials of the satellite are small because of the low geomagnetic field at the altitudes of interest and because of the satellite's low angular speed. The torques due to self-gravity and eddy currents are less than 10^{-8} ft-lb. The torques produced by plasma effects due to the motion of the satellite in the Van Allen radiation belts are believed to be small. However, it is intended to make a detailed analysis of plasma effects.

8.7 *Summary*

In Table VIII, the maximum libration angles are summarized for each individual disturbance for the high-deck configuration. By simply superposing the individual effects of the various torques, the maximum steady-state libration amplitude is about 10° for the high-deck configuration. However, the various maximum individual effects cannot simply be added to obtain expected maximum libration amplitude. For example, the effect of solar torque and solar rod bending are not additive. The solar torque causes the deck assembly to rotate about the center of mass of the composite satellite in a direction away from the sun, whereas the rod bending due to solar heating causes an effect in the opposite direction. A quantitative analysis is being made of the compensating effects

TABLE VIII — EFFECTS OF DISTURBANCES FOR A 6000-NM SYSTEM

Sources	Maximum Magnitude (ft-lb)	Approximate Librational Angle
Pitch gravity torque: 1.3×10^{-5} per degree off the local vertical		
Solar radiation*	5×10^{-5}	4°
Rod deflection*	See text	
Natural bending		1.5°
Solar heating		3.0°
Orbital eccentricity	See text	1.5° for $\epsilon = 0.005$
Magnetic dipole moment	0.48×10^{-5}	0.4°
Self-gravity and eddy current	Negligible	Negligible

Effects* of Meteorite Impact		
Angle from the Local Vertical	$\hat{N}$, Expected Number of Occurrences per Year	Period of Occurrence in Years
5°-15°	0.336	3
15°-30°	0.082	24
30°-50°	0.031	33
50°-70°	0.011	94
70°-90°	0.003	355
5°-90°	0.460	2
>90° (turnover or tumbling)	0.044	23

* Computed for high-deck configuration.

of these two disturbances. Should it develop that the disturbances do not substantially compensate for each other, silver-plating the rods would reduce the effects of both disturbances to less than 5°, rather than 7°, which is the sum of the two disturbance angles. The effects of the other disturbances — natural rod bending, orbit eccentricity, magnetic dipole moment — would not be added to give a total angle of 3.4°. Hence for the high-deck configuration, the final librational angle is expected to be well under 10°. For the low-deck configuration, the librational angle would be expected to be somewhat smaller than that for the high-deck configuration.

IX. CONCLUSIONS

The theoretical feasibility of the proposed PGAC system has been amply demonstrated by more than one hundred computer runs based on the dynamics analysis[4] of the ideal two-rigid-body system. Computer simulations made with a wide variety of initial conditions showed that the system stopped tumbling and then, within about 7 orbital periods, settled down to a state of small oscillations about an earth-pointing direction. It has also been indicated that disturbing influences, such as solar radiation pressure and orbital eccentricity, produce oscillations of less than 10° for a 6000-nm orbit.

The rods have been shown to possess adequate rigidity, to be fully capable of withstanding the loads imposed during the extension phase, and not to undergo excessive bending due to solar heating.

On the basis of comprehensive studies and tests, it is believed that the PGAC system described in this paper is fully capable of meeting all its design objectives, including compatibility with multiple launch procedures, and that it will provide a significant advance in communications satellites practice.

X. ACKNOWLEDGMENTS

The authors wish to acknowledge fully the technical contributions of L. Rongved* and his leadership during the formative stages of the project; H. J. Fletcher* also contributed numerous ideas and mathematical results. Among present Members of Staff at Bell Telephone Laboratories the authors are indebted to J. G. Engstrom, J. W. Stafford, and B. A. Unger who contributed greatly to various analytical and experimental investigations, to L. S. Goldmann who contributed to Section 3 2, and to R. G. Murray for assistance in certain test proce-

* Now with Bellcomm, Inc.

dures. Thanks are also due to Miss E. B. Murphy, Mrs. C. M. Kimme, and Mrs. W. L. Mammel for programming various computations on the IBM 7090 computer.

REFERENCES

1. Hoth, D. F., O'Neill, E. F., and Welber, I., The *Telstar* Satellite System, B.S.T.J., **42**, July, 1963, p. 765.
2. Kamm, L. J., An Improved Satellite Orientation Device, ARS Journal, **32**, No. 6, 1962, pp. 911–913.
3. Fischell, R. E., The TRAAC Satellite, APL Technical Digest, **1**, No. 3, 1962, pp. 2–9.
4. Fletcher, H. J., Rongved, L., and Yu, E. Y., Dynamics Analysis of a Gravitationally Oriented Satellite, this issue, pp. 2239–2266.
5. Nowak, G. H., et al., Unclassified Study of Vertistat Orientation for Communication Satellites, Final Report, Contract NAS5-1898. GD/A Report No. AE 62-0808, 15, September, 1962.
6. Paul, B., Planar Librations of an Extensible Dumbbell Satellite, AIAA Journal, Vol. 1, No. 2, 1963, pp. 411–418.
7. Pierce, J. R., Orbital Radio Relays, Jet Propulsion, **25**, 1955, pp. 153–157.
8. Timoshenko, S., and Young, D. H., *Vibration Problems in Engineering*, D. Van Nostrand, Princeton, N. J., 3rd ed., 1955.
9. Heydon, D. A., Final Report, OGO/Agena B, Separation System Development Tests, STL Document No. 2319-6029-TU-000, 9521.23-128, 26 December, 1962.
10. Aichroth, W. W., Test Report OGO Separation Test, 19V–21, STL Doc. No. 2319-6030-TU-000, 7 January, 1963.
11. Warren, H. R., DeHavilland Antenna Erection Unit, Proc. 5th MIL-E-CON Conference, IRE, 1961, pp. 392–400.
12. Charnes, A., and Raynor, S., Solar Heating of a Rotating Cylindrical Space Vehicle, ARS Journal, **30**, No. 5, May, 1960, pp. 479–484.
13. Timoshenko, S., and Goodier, J. N., *Theory of Elasticity*, McGraw-Hill, New York, 1951, pp. 399–404.
14. Rinehart, J. D., and Robbins, M. F., Characteristics of the Service Provided by Communication Satellites in Uncontrolled Orbits, B.S.T.J., **41**, September, 1962, pp. 1621–1670.
15. Timoshenko, S., *Strength of Materials*, Part I, D. Van Nostrand, Princeton, N. J., 3rd ed., 1958, p. 313.
16. Timoshenko, S., *Strength of Materials*, Part II, D. Van Nostrand, Princeton, N.J., 3rd ed., 1959.
17. Paul, B., A Modification of the Coulomb-Mohr Theory of Fracture, Jour. Appl. Mech., **28**, June, 1961, pp. 259–268.
18. Lewis, J. A., Viscous Damping of Gravitationally Stabilized Satellites, Proc. 4th U.S. Nat. Congr. Appl. Mech., Berkeley, June 18–21, 1962, Am. Soc. Mech. Engrs., 1962, pp. 251–254.
19. Zajac, E. E., Damping of a Gravitationally Oriented Two-Body Satellite, ARS Journal, **32**, December, 1962, pp. 1871–1875.
20. Yu, E. Y., Long Term Coupling Effects between Librational and Orbital Motions of a Satellite, to be published.
21. Whipple, F. L., The Meteoritic Risk to Space Vehicles, in *Vistas in Astronautics*, **1**, M. Halperin and M. Stern, Eds., Pergamon Press, New York, 1958.
22. Dubin, M., IGY Micrometeorite Measurements, in *Space Research*, H. Kallmann, Ed., North-Holland Publ. Co., Amsterdam, 1960, pp. 1042–1058.